Dimer of substitutional carbon in silicon studied by EPR and *ab initio* methods

J. R. Byberg
Institute of Chemistry, University of Aarhus, DK-8000, Denmark

B. Bech Nielsen and M. Fanciulli*
Institute of Physics and Astronomy, University of Aarhus, DK-8000, Denmark

S. K. Estreicher
Department of Physics, Texas Tech University, Lubbock, Texas 79409-1051

P. A. Fedders
Department of Physics, Washington University, St. Louis, Missouri 63130-1105
(Received 31 August 1999)

An EPR signal observed in carbon-doped float-zone silicon after irradiation with 2-MeV electrons at room temperature has been investigated. It represents a defect with $S=\frac{1}{2}$, an apparently isotropic g factor ($=2.0030$), and a complicated hyperfine structure from ^{29}Si nuclei in five shells that are consistent with an overall trigonal symmetry. Subtle asymmetries of the hyperfine pattern indicate the presence of a small trigonal component of the g tensor as well. An additional pair of satellite lines is identified by the relative intensity (1%) as arising from ^{13}C in natural abundance, occupying two equivalent sites on the trigonal axis. Several defect structures that contain two equivalent carbon atoms on a trigonal axis were investigated by *ab initio* Hartree-Fock calculations. Only the negative charge state of a dicarbon center C_s-C_s, in which the carbon atoms occupy adjacent substitutional sites, was found to be consistent with the EPR data.

I. INTRODUCTION

Carbon is an important impurity in silicon, which may strongly influence the course of radiation-induced processes in this material. Thus substitutional carbon (C_s) effectively traps the self-interstitial (Si_i) thereby forming a silicon-carbon $\langle 100\rangle$ split-interstitial denoted C_i.[1] C_i becomes mobile in the lattice slightly above room temperature and may become trapped at substitutional carbon. The resulting metastable complex C_s-C_i has been studied in great detail.[2–4] The mere fact that carbon atoms come close together during electron irradiation of carbon-doped silicon near room temperature opens the possibility that other types of dicarbon defects could also arise. In the present work one such defect has been detected by the associated electron paramagnetic resonance (EPR) signal. The observed properties of the new dicarbon defect combined with the results of *ab initio* Hartree-Fock calculations strongly indicate that the carbon atoms occupy adjacent substitutional sites, and the defect is accordingly labeled C_s-C_s. The structure involves a direct carbon-carbon bond, thus contrasting that of C_s-C_i, in which the carbon atoms are linked through a bridging silicon atom.

II. EXPERIMENTAL METHODS

A. Sample preparation

The samples used in this study were all *n*-type float-zone silicon doped with carbon having the natural composition of isotopes, 98.9% ^{12}C and 1.1% ^{13}C. The carbon concentration was about 3×10^{17}, and the content of phosphorus was in the range 1×10^{15}–$5\times10^{16}\,\mathrm{cm}^{-3}$. A set of samples was, in addition, doped with tin enriched to 87% ^{119}Sn at a concentration level of $10^{18}\,\mathrm{cm}^{-3}$. A typical sample had a volume of about $2\times4\times6\,\mathrm{mm}^3$.

The samples were mounted inside a vacuum chamber with a background pressure of about 10^{-5} torr on a copper block attached to the cold stage of a closed-cycle helium cryocooler, and irradiated with 2-MeV electrons to a typical dose of about $10^{18}\,\mathrm{cm}^{-2}$. The temperature on the copper block was monitored during the irradiation, and the electron flux was chosen so that the block temperature was always within the limits 300–380 K. During the irradiation the electron beam was swept horizontally and vertically to ensure a homogeneous lateral distribution of defects.

B. Equipment

The EPR spectra were recorded with a Bruker ESP 300E spectrometer operated at *X* band (9.3–9.5 GHz) in the absorption mode. The static magnetic field was modulated at 100 kHz, except when resolution enhancement via third-harmonic detection was employed.[5,6] In that case the field was modulated at 33 kHz, while the EPR signal was detected at 100 kHz. The microwave frequency ν_0 and the magnetic field $\mathbf{B}_0$ were monitored continuously with an electronic counter and a NMR gaussmeter. Sample temperatures in the range 3–300 K were obtained with an APC Heli-trans liquid-helium flow cryostat. The samples were glued with epoxy resin to a silver rod that was screwed into the cold block of the cryostat, and thermally shielded by a thin-walled, silvered brass tube. A quartz tube (10 mm in diameter) serving as a vacuum shroud allowed the sample to be centered in the cylindrical room-temperature cavity. The samples were

mounted on a face coinciding with the $(1\bar{1}0)$ plane, i.e., with the $[1\bar{1}0]$ crystal axis along the axis of the cryostat-cavity assembly, around which the magnet could be rotated. Those samples containing tin displayed a strong EPR signal from SnV^0 (G29).[7] Because this signal is extremely anisotropic, $\mathbf{B}_0$ could be aligned with any of the main axes of the sample ([001], [110], and [111]) to within 0.05°.

C. Analysis of spectra

The spin Hamiltonian parameters representing the EPR signal discussed below were derived from the line positions measured at 200 K for $\mathbf{B}_0$ aligned with the three major axes, by means of computer simulations of the entire signal. The hyperfine tensors describing the satellite lines arising from ^{29}Si nuclei were taken from the outset to be axial and, except for one set of equivalent silicon sites, with the unique axis along a ⟨111⟩ direction. Hence only two parameters per hyperfine tensor, rather than six, had to be fitted to the spectra. This proved to be an adequate approximation.

III. EXPERIMENTAL RESULTS

A. EPR signal of the dicarbon defect

In a recent EPR study of defects in *n*-type silicon doped with tin and carbon, an almost isotropic EPR signal, consisting of a strong central line and two pairs of fairly intense satellite lines, was observed after heavy irradiation with 2-MeV electrons at room temperature.[8] We have now observed the same signal in a set of *n*-type samples doped with carbon but containing no tin. We can therefore rule out the involvement of tin in the associated defect, although the best signal-to-noise ratio was obtained in the tin-doped samples. The signal represents a defect with electron spin $S=\frac{1}{2}$. The *g* value (2.0030) and the separation and relative intensities of the satellites all agree with those reported 30 years ago for an unidentified, cubic EPR signal labeled GGA-2,[9] which was observed in *n*-type (phosphorus-doped) silicon after irradiation with 30-MeV electrons at room temperature. We therefore adopt the label GGA-2 for the signal observed in our samples.

The two pairs of intense satellite lines, which depend only slightly on the orientation of $\mathbf{B}_0$, may be ascribed reasonably to hyperfine interaction with ^{29}Si nuclei in many equivalent positions. Owing to their natural abundances, neither of the other possible candidates, ^{13}C and ^{31}P, is a likely source of these satellites. However, the very good signal-to-noise ratio for the samples containing tin allowed the detection of a set of weak satellite lines corresponding to a strongly anisotropic hyperfine tensor with trigonal symmetry. When $\mathbf{B}_0$ is directed along [001], these satellites therefore coalesce into one pair of weak replicas of the central GGA-2 signal, each replica having a relative signal height of 0.011 ± 0.001 (see Fig. 1, curve *a*). Owing to the very accurate alignment (0.05°) attained via the SnV^0 signal, the observed heights are proportional to the relative intensities to a very good approximation despite the markedly different angular variations of satellites and the central signal. The observed relative intensity of the weak satellites shows that they cannot arise from hyperfine interaction with ^{29}Si nuclei: Since the natural abundance of this isotope is 4.67% and its nuclear spin is $I=\frac{1}{2}$, an electron-spin density at a single silicon site will result in a pair of satellite lines with a relative intensity of 0.024 rather than 0.011 as observed. Moreover, if the satellites were assumed to arise from defects containing *two* ^{29}Si nuclei in a shell of *n* equivalent silicon sites, then defects containing just one ^{29}Si in that shell should yield two replicas of the central signal with relative height close to 0.15 and separated by half the distance between the weak second-order replicas. As can be seen in Fig. 1, curve *a*, no such strong replicas exist. Instead we assign the weak satellites to ^{13}C. This is the only stable isotope of carbon with nonzero spin ($I=\frac{1}{2}$) and, since the natural abundance is 1.11%, a hyperfine interaction with ^{13}C occupying two equivalent carbon sites will give rise to a pair of satellite lines of precisely the observed relative intensity. In order to yield the observed signal for all directions of $\mathbf{B}_0$, the two carbon sites must be magnetically indistinguishable. Moreover, the trigonal symmetry of the hyperfine tensor (common to both sites) indicates that the carbon atoms are both located on the [111] symmetry axis. The principal values of the hyperfine tensor $\mathbf{A}(^{13}\mathrm{C})$ are given in Table I. Interpreted within the conventional model of linear combination of atomic orbitals by means of the hyperfine coupling constants associated with the $2s$ and $2p$ atomic orbitals of carbon,[10] the hyperfine parameters yield the spin populations $\rho_{2s}(\mathrm{C})=0.024$ and $\rho_{2p}(\mathrm{C})=0.28$ on each of the two carbon atoms, if the principal values of $\mathbf{A}(^{13}\mathrm{C})$ are assumed to have the same sign. If opposite signs are assumed, we obtain $\rho_{2s}(\mathrm{C})$

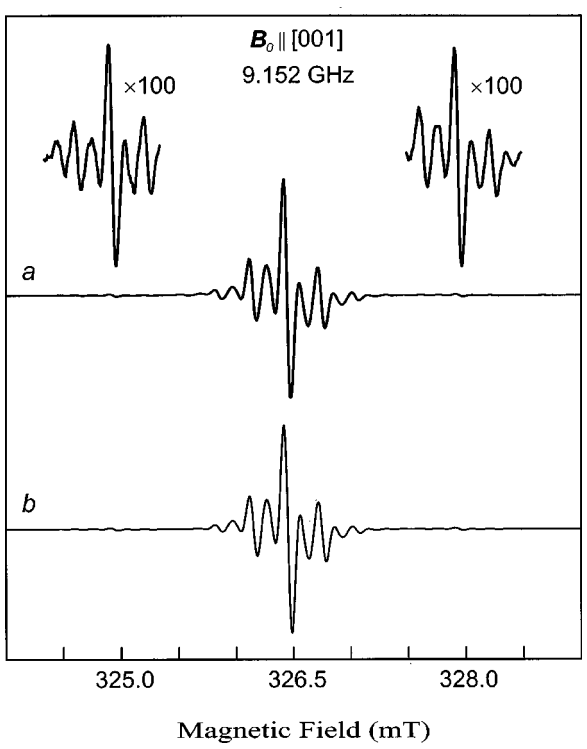

FIG. 1. Curve *a*: GGA-2 signal recorded at 200 K with $\mathbf{B}_0$ along [001]. Strong satellites close to the central line arise from hyperfine interaction with ^{29}Si nuclei in five shells, whereas the weak replicas of the central group with relative intensity 0.011 reflect the interaction with ^{13}C nuclei in two equivalent positions. Curve *b*: Simulation of the signal calculated from the parameters in Table I and a Gaussian line shape with a peak-to-peak width of 0.07 mT.

TABLE I. Spin Hamiltonian parameters for the GGA-2 signal $[(C_s\text{-}C_s)^-]$. All terms are axial with the unique axis denoted *Z*. Principal values $A_\parallel$ and $A_\perp$ of $\mathbf{A}(^{13}C)$ and $\mathbf{A}_n(^{29}Si)$ are given in MHz. The same sign is *assumed* for $A_\parallel$ and $A_\perp$, corresponding to a positive net spin density at all nuclei. Limits of error: *g*, ± 0.0001; $g_\parallel - g_\perp$, $\pm 0.000\,01$; $A(^{13}C)$, ± 1 MHz; and $A_n(^{29}Si)$, ± 0.2 MHz.

Term	(∥) value	(⊥) value	*Z*	No. of sites
g	2.00309	2.00300	[111]	
$A(^{13}C)$	129.3	47.6	[111]	2
$A_1(^{29}Si)$	−21.3	−14.1	[111]	6
$A_2(^{29}Si)$	−17.5	−16.7	[111]	6
$A_3(^{29}Si)$	−11.2	−7.9	$[\bar{1}11][1\bar{1}1][11\bar{1}]$	two each
$A_4(^{29}Si)$	−6.0	−7.3	$Z\perp [1\bar{1}0][10\bar{1}][01\bar{1}]$ $\angle(Z,[111])=37°$	four each
$A_5(^{29}Si)$	−2.3	−1.6	[111]	~8

$=0.003$ and $\rho_{2p}(C)=0.55$. In either case a substantial fraction of the electron spin is localized on the two carbon atoms.

B. ^{29}Si hyperfine splittings

As noted already, the pattern of strong satellite lines in the GGA-2 signal suggests hyperfine interactions with ^{29}Si nuclei occupying sets of equivalent sites. The shape of the satellite lines is somewhat asymmetric (see Fig. 1), which indicates that the observed lines in fact consists of unresolved, discrete components. This was borne out by recording the signal with resolution enhancement, as illustrated in Fig. 2, curves *a*, *b*, and *c*, for $\mathbf{B}_0$ along the three main axes. A substantial number of hyperfine lines are now resolved. The hyperfine pattern of the signal recorded with $\mathbf{B}_0$ parallel to [001] (curve *a*) is symmetric about the central line. In contrast, those observed for $\mathbf{B}_0$ along the other two major axes are clearly asymmetric, which immediately shows that the *g* factor cannot be strictly isotropic. The curves labeled *a′*, *b′*, and *c′*, in Fig. 2 are simulations obtained with five sets of axial hyperfine tensors $\{\mathbf{A}_i(^{29}Si)\}$, $i=1-5$, given in Table I, and with the assumption that the corresponding ^{29}Si nuclei belong to shells containing six, six, six, 12, and 8 equivalent silicon sites. In addition, a small trigonal component of the *g* tensor was introduced to account for the asymmetries observed for $\mathbf{B}_0$ along [111] and [110]. The sets $\{\mathbf{A}_1(^{29}Si)\}$ and $\{\mathbf{A}_2(^{29}Si)\}$ both have their common unique axis directed along the trigonal axis [111], whereas the axes of $\{\mathbf{A}_3(^{29}Si)\}$ points along $[\bar{1}11]$, $[1\bar{1}1]$, or $[11\bar{1}]$, and the tensors of the set $\{\mathbf{A}_4(^{29}Si)\}$ are monoclinic *I* with the unique axes inclined at 37° to the [111] direction. As is apparent from the fit to the experimental curves, the axial tensors $\mathbf{A}_i(^{29}Si)$ yield an adequate representation of the hyperfine pattern. We note, however, that while the first four sets of tensors could be unambiguously determined apart from the signs of $A_\perp$ and $A_\parallel$, $\{\mathbf{A}_5(^{29}Si)\}$, the numbers of sites in the fifth shell must be considered as crude estimates only, because the shape of the satellites closest to the main lines may be distorted by the resolution-enhancement procedure. The total spin population in silicon $3s$ and $3p$ orbitals, estimated from the values of $A_\perp(^{29}Si)$ and $A_\parallel(^{29}Si)$ all taken with the same sign, is $\rho(Si)=0.31$.

C. Symmetry of the dicarbon defect

All terms in the spin Hamiltonian for the dicarbon defect are consistent with a defect symmetry as high as D_{3d}. However, since the derivation was based on EPR spectra obtained at 200 K to avoid interference with other signals emerging at lower temperatures, the observed symmetry might conceivably arise from swift jumps of the defect among equivalent configurations around the trigonal axis. To check this possibility, we monitored the signal for $\mathbf{B}_0$ parallel to [100] right down to 3.3 K. No splitting of the central line was observed,

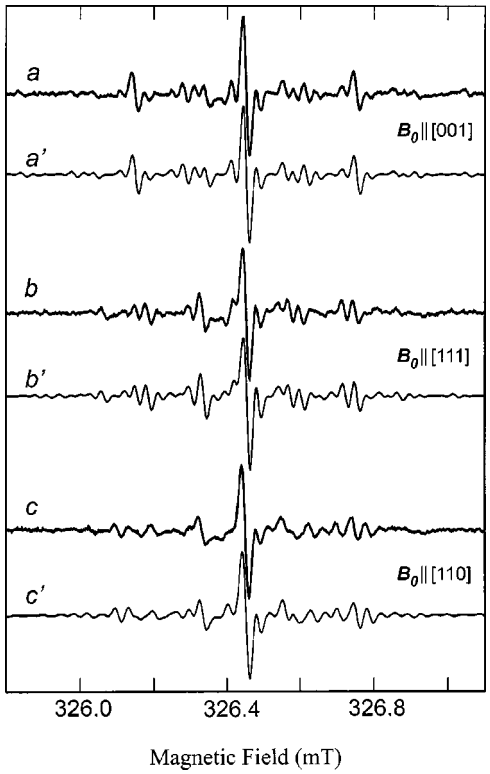

FIG. 2. GGA-2 signal recorded with third-harmonic detection for $\mathbf{B}_0$ aligned with the three main axes (curves *a*, *b*, and *c*). The hyperfine pattern of curve *a* is symmetric with respect to the central line, whereas those of curves *b* and *c* are asymmetric, indicating a small trigonal anisotropy of the *g* factor. Curves *a′*, *b′*, and *c′* are simulations calculated from the parameters of Table I and a Gaussian line shape with a peak-to-peak width of 0.018 mT.

from which we infer that the trigonal symmetry seen at 200 K is retained to within the spectral resolution. This strongly indicates that the trigonal symmetry characterizes the ground state of the defect rather than results from a thermally activated process. We note, however, that the observations do not exclude that rapid tunneling among nontrigonal configurations could occur.

IV. STRUCTURE OF THE DICARBON DEFECT

The simplest structure consistent with the observed EPR signal described above is a pair of carbon atoms occupying adjacent substitutional sites, which we label C_s-C_s. However, there are several alternative structures containing two carbon atoms on a trigonal axis and sets of six or 12 equivalent silicon atoms in surrounding shells. These include (a) two substitutional carbon atoms in a ring hexavacancy[11,12] replacing the two silicon atoms on its trigonal axis, and (b) two interstitial carbon atoms on the trigonal axis of the hexavacancy, which we label C_s-V_6-C_s and C_i-V_6-C_i, respectively. Both structures could in principle give rise to the observed EPR signal, and were therefore investigated together with C_s-C_s by means of *ab initio* Hartree-Fock (HF) theory. The geometries were energy optimized at one or more levels of theory and the electronic structures calculated.

A. Theoretical methods

The geometries were first energy optimized at an approximate *ab initio* HF level with the PRDDO method.[13,14] This technique reproduces, at a fraction of the cost, the results of *ab initio* HF calculations with minimal basis sets. Hydrogen-saturated silicon clusters with 38 or 44 silicon atoms were used. The geometries were optimized by a gradient method without symmetry restrictions. The two carbon atoms and all the silicon atoms adjacent to the carbon atoms or to the hexavacancy were allowed to move during the optimization.

For all complexes the calculations were first performed for the neutral charge state with a restricted (closed-shell) wave function. After energy optimization only C_s-C_s and C_s-V_6-C_s retained trigonal symmetry, and both had an empty one-electron level within the silicon band gap. These two defects were energy optimized again in the positive and the negative charge states by means of an unrestricted HF wave function and clusters with a net charge of $+e$ and $-e$, respectively. The PRDDO results were used as inputs for further calculations at the *ab initio* HF level. These calculations were carried out with pseudopotentials, split-valence basis sets on all atoms, and polarization functions on those host atoms that were allowed to relax.[15] Additional geometry optimization at this level were performed in the same cluster, but now with trigonal symmetry imposed. The structures obtained with the PRDDO and *ab initio* HF methods agree well. The findings described below were obtained from the *ab initio* HF calculations.

In the discussion of the results we take advantage of the quantum-chemical approach, which provides details about the chemical interactions via standard Mulliken population analysis.[16] In addition to single-electron orbital occupancies, one obtains *overlap populations* (positive when the two atoms form a covalent bond, and negative otherwise), the *degree of bonding*[17] (ranging from zero for a purely ionic bond to unity for an ideal two-electron covalent bond), and the *spin densities* in each atomic orbital or summed over atoms.

The results for C_s-C_s were also tested in a 128-atom supercell using an *ab initio* tight-binding molecular-dynamics approach[18] based on density-functional theory. For the neutral charge state, the results closely agree with those obtained from *ab initio* HF calculations. An attempt was made to simulate *n*-type material by substituting a phosphorus atom for a silicon atom in the supercell. However, the additional electron did not become trapped on the two carbon atoms, but remained at the phosphorus atom.

B. Ring hexavacancy with two carbon atoms

As noted above, the configuration C_s-V_6-C_s, with two carbon atoms substituted for two silicon atoms on the trigonal axis of V_6, retained the trigonal symmetry after optimization. This defect has several localized one-electron states within the band gap, and could therefore trap or emit an electron. However, the two carbon atoms end up too far from each other to overlap covalently. The C-C distance is 5.52 Å, which exceeds the equilibrium distance for a normal C-C bond length by almost a factor of 4. In the negative or positive charge state, the unpaired electron resides in an orbital attached to just one of the carbon atoms. Thus, the two carbon atoms are inequivalent in contrast to the experimental observations. The two carbon atoms of C_i-V_6-C_i are no longer located on the trigonal axis after optimization. Therefore, we conclude that neither C_s-V_6-C_s nor C_i-V_6-C_i can account for the GGA-2 signal.

C. C_s-C_s pair

In the calculation of the structure of the C_s-C_s defect, the two carbon atoms were at the outset placed on adjacent lattice sites. After relaxation of the carbon atoms and their nearest silicon neighbors, the D_{3d} symmetry of the defect was retained for the charge states $(C_s\text{-}C_s)^0$ and $(C_s\text{-}C_s)^-$. However, in $(C_s\text{-}C_s)^+$ the two carbon atoms became inequivalent (point group C_{3v}). The structures obtained are shown in Fig. 3. In the neutral charge state, the carbon-carbon distance is 2.08 Å, which is again substantially larger than the normal C-C bond length. However, the degree of bonding is 0.48 and the overlap population is $+0.38$, which demonstrates that there is considerable covalent bonding. The Si-C bond length is 2.07 Å, which significantly exceeds the length of a normal Si-C bond ($\sim$1.9 Å). The calculated spectrum of one-electron energies for a neutral cluster containing a C_s-C_s unit at the center is compared to that of a perfect cluster in Fig. 4. As can be seen from the figure, $(C_s\text{-}C_s)^0$ has an unoccupied level in the upper half of the band gap.[19] The associated wave function closely resembles an antibonding combination of the carbon orbitals engaged in the C-C bond. For a normal C-C bond, the bonding/antibonding energy separation greatly exceeds the silicon band gap. However, in C_s-C_s the two carbon atoms are forced apart by the six stretched Si-C bonds. Hence the bonding/antibonding energy difference is significantly reduced in $(C_s\text{-}C_s)^0$, which lowers the one-electron energy of the (unoccupied) antibonding orbital to below the conduction-band edge.

When an electron is added to the cluster, it enters the antibonding C_s-C_s orbital, and the defect becomes EPR ac-

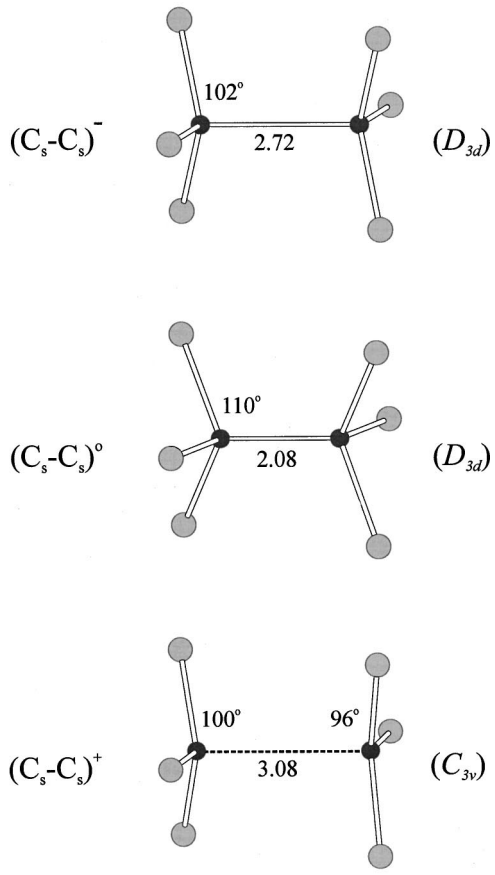

FIG. 3. Equilibrium configurations of $(C_s\text{-}C_s)^-$, $(C_s\text{-}C_s)^0$, and $(C_s\text{-}C_s)^+$ obtained from *ab inito* HF theory on a 44-atom silicon cluster. The internuclear distances are given in Å, and the bond angles (∠C-C-Si) in degrees. The carbon atoms are black, whereas the silicon atoms are light gray.

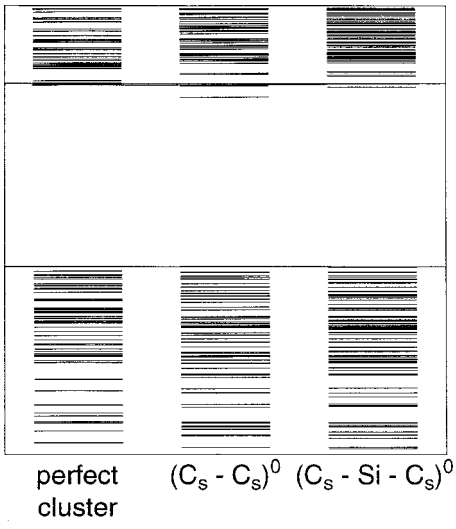

FIG. 4. One-electron energies calculated with *ab initio* HF theory for (a) the perfect 44-atom silicon cluster, (b) the silicon cluster with $(C_s\text{-}C_s)^0$, and (c) the silicon cluster with $(C_s\text{-Si-}C_s)^0$. The lowest-lying unoccupied state of $(C_s\text{-}C_s)^0$ is associated with an antibonding orbital localized on the carbon atoms. Note that the energies of the unoccupied states are not directly comparable to gap levels.

tive. Populating the antibonding orbital weakens the C-C bond, so that the two carbon atoms move further apart, and the Si-C bonds shorten. The energy-optimized structure of $(C_s\text{-}C_s)^-$ has a C-C separation of 2.72 Å, which is nearly twice the normal bond length, and a Si-C distance of 1.95 Å. Even at this large C-C separation, the bond is not completely broken, as evidenced by a positive, although small, overlap population (+0.03). The bonding orbital still has a lower energy than the antibonding orbital, and the spin populations on the two carbon atoms remain identical. The calculated electron-spin distribution spreads over the two carbon atoms as well as the neighboring silicon atoms. The atomic spin populations are +0.84 on each carbon atom, −0.16 on the six nearest neighbors, and +0.12 on six of the 12 second-nearest neighbors. The very strong spin polarization suggested by this result is probably an artifact often encountered in unrestricted HF calculations,[20] whereas the high degree of spin localization on the carbon atoms is expected to be real. Hence the properties calculated for $(C_s\text{-}C_s)^-$ are all in accordance with those observed for the GGA-2 center.

Like $(C_s\text{-}C_s)^-$, the positive charge state $(C_s\text{-}C_s)^+$ may be observable by EPR. This charge state also has a large C-C separation because the bonding orbital is only occupied by one electron. In fact, the C-C distance obtained for $(C_s\text{-}C_s)^+$ is even larger than in $(C_s\text{-}C_s)^-$. Accordingly, the overlap population in $(C_s\text{-}C_s)^+$ is only +0.005, showing that the C-C bond is essentially broken. Consequently, the two carbon atoms are inequivalent in this charge state, and the unpaired electron spin is entirely localized on one carbon with zero net spin on the other. Since the observed properties of the GGA-2 center are inconsistent with these findings, we rule out $(C_s\text{-}C_s)^+$ as the origin of the EPR signal.

Although our calculations show that $C_s\text{-}C_s$ can exist in silicon, this configuration does not represent the global energy minimum for two substitutional carbon atoms in that material. This was demonstrated by a calculation on the complex $(C_s\text{-Si-}C_s)^0$, which consists of two carbon atoms at second-nearest substitutional sites. The total energy of this defect was found to be 1.4 eV below that of $(C_s\text{-}C_s)^0$. Hence $(C_s\text{-}C_s)^0$ represents a metastable state for two substitutional carbon atoms, but with an energy barrier large enough, to prevent spontaneous dissociation into two C_s^0 at next-nearest or more distant substitutional sites.

D. Assignments

On the basis of the results described above, we assign the GGA-2 signal to $(C_s\text{-}C_s)^-$. It follows from this assignment that the unpaired electron spin occupies an antibonding combination of dangling-bond-like orbitals centered on the two carbon atoms. With the assumption that $A_\parallel(^{13}C)$ and $A_\perp(^{13}C)$ are both positive, the spin population estimated for each of these ''dangling bonds'' is 0.3, which is about half the spin population estimated similarly from the largest ^{29}Si hyperfine tensor for an isolated silicon dangling bond on the Si/SiO_2 interface (the P_b center).[21] Assuming that the spin density spreads over the silicon atoms *behind* the carbon atoms of the GGA-2 center in much the same way as it projects backwards from a silicon atom carrying a dangling bond,[22] we may attempt to assign the ^{29}Si hyperfine splittings to specific silicon sites by comparison with the P_b cen-

ter. Detailed calculations[22] on this defect have shown that the largest ^{29}Si hyperfine interaction (apart from that associated with the atom carrying the dangling bond itself) stems from three of the second-nearest neighbors, and has its axis aligned almost perfectly with the dangling-bond axis ([111]). The net spin population on the three nearest neighbors is small because the contributions from direct overlap and spin polarization nearly cancel. Furthermore, the resulting hyperfine tensors at these sites have their unique axes directed approximately along $[\bar{1}11]$, $[1\bar{1}1]$, and $[11\bar{1}]$. The hyperfine tensors of the second-nearest neighbors of the P_b center have the principal values $A_{\|}(^{29}\mathrm{Si}) = -42.6\,\mathrm{MHz}$ and $A_{\perp}(^{29}\mathrm{Si}) = -34.9\,\mathrm{MHz}$.[21] Scaled with the ratio (0.5) of the spin populations in the carbon and silicon dangling-bond orbitals, these values yield a surprising (perhaps fortuitous) agreement with $\mathbf{A}_1(^{29}\mathrm{Si})$ of GGA-2 (Table I). Hence we assign $\mathbf{A}_1(^{29}\mathrm{Si})$ to the six silicon atoms in second-nearest-neighbor positions to the carbon atoms, labeled 1 in Fig. 5. Moreover, we assign the set of six equivalent hyperfine tensors $\{\mathbf{A}_3(^{29}\mathrm{Si})\}$ to the six nearest neighbors (labeled 3). The analysis of the hyperfine splittings of the P_b center provides no further guidance. It seems reasonable, however, to assign the set of 12 equivalent tensors $\{\mathbf{A}_4(^{29}\mathrm{Si})\}$ to the twelve second-nearest neighbors labeled 4, and the six tensors $\{\mathbf{A}_2(^{29}\mathrm{Si})\}$ to the set of third-nearest neighbors labeled 2, which are almost as close to the carbon atoms as the second-nearest neighbors (1). It may be noted that despite the similar numerical ''sizes'' of $\mathbf{A}_1(^{29}\mathrm{Si})$ and $\mathbf{A}_2(^{29}\mathrm{Si})$, the corresponding spin populations have a ratio 4:1.

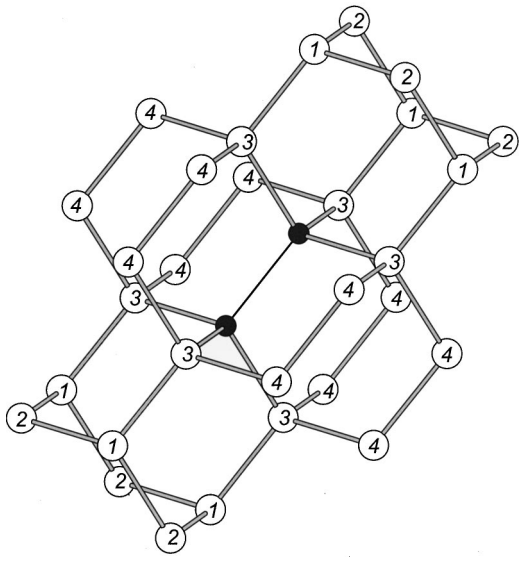

FIG. 5. Sketch of the structure of $(C_s\text{-}C_s)^-$, showing the silicon sites thought to give rise to the hyperfine splittings described by the tensors $\mathbf{A}_n(^{29}\mathrm{Si})$, $n=1,...,4$. Note that the largest splitting $[\mathbf{A}_1(^{29}\mathrm{Si})]$ is assigned to a set of second-nearest neighbors to the carbon atoms.

V. CONCLUSIONS

A carbon dimer C_s-C_s in crystalline silicon has been identified. The defect consists of two carbon atoms at adjacent substitutional sites. In the negative charge state, observed by EPR, the carbon atoms are displaced symmetrically along the trigonal axis, attaining a separation which is nearly twice the normal C-C bond length in molecules. However, the two carbon atoms remain covalently bonded together, allowing a symmetrical distribution of the unpaired electron spin in the C_s-C_s antibonding orbital. In the neutral charge state the defect also has D_{3d} symmetry, but the C-C bond is much shorter than in the negative charge state. C_s-C_s represents a local, rather than a global, minimum in the potential-energy surface of two substitutional carbon atoms in silicon, and, in that sense, the defect is metastable.

ACKNOWLEDGMENTS

This work was supported by the Danish National Research Foundation through the Aarhus Center for Atomic Physics (ACAP). S. K. Estreicher acknowledges Grant No. D-1126 from the R. A. Welch Foundation and Contract No. XAD-7-17652-01 from the National Renewable Energy Laboratory. The assistance of Peter Johannesen in the preparation of several figures is gratefully acknowledged.

*Present address: Laboratorio MDM-INFM, Agrate Brianza (MI), I-20041, Italy.

[1] G. D. Watkins and K. L. Brower, Phys. Rev. Lett. **36**, 1329 (1976).
[2] L. W. Song, X. D. Zhan, B. W. Benson, and G. D. Watkins, Phys. Rev. Lett. **60**, 460 (1988).
[3] L. W. Song, B. W. Benson, and G. D. Watkins, Appl. Phys. Lett. **51**, 1155 (1987).
[4] E. V. Lavrov, L. Hoffmann, and B. Bech Nielsen, Phys. Rev. B **60**, 8081 (1999).
[5] S. H. Glarum, Rev. Sci. Instrum. **36**, 771 (1965).
[6] L. C. Allen, H. M. Gladney, and S. H. Glarum, J. Chem. Phys. **40**, 3135 (1964).
[7] G. D. Watkins, Phys. Rev. B **12**, 4383 (1975).
[8] M. Fanciulli and J. R. Byberg, Phys. Rev. B (to be published).
[9] H. Horiye and E. G. Wikner, J. Appl. Phys. **40**, 3879 (1969).
[10] J. R. Morton and K. F. Preston, J. Mater. Res. **30**, 577 (1978).
[11] S. K. Estreicher, J. L. Hastings, and P. A. Fedders, Appl. Phys. Lett. **70**, 432 (1997).
[12] J. L. Hastings, S. K. Estreicher, and P. A. Fedders, Phys. Rev. B **56**, 10 215 (1997).
[13] A. Derecskei-Kovacs and D. S. Marynick, Int. J. Quantum Chem. **58**, 193 (1996).
[14] A. Derecskei-Kovacs, D. E. Woon, and D. S. Marynick, Int. J. Quantum Chem. **61**, 67 (1997).
[15] M. W. Schmidt, K. K. Baldridge, J. A. Boats, S. T. Elbert, M. S. Gordon, J. H. Jensen, S. Koseki, K. A. Nguyen, S. Su, T. L. Windus, M. Dupuis, and J. A. Montgomery, Jr., J. Comput. Chem. **14**, 1349 (1993).
[16] W. A. Hehre, L. Radom, P. v.R. Schleyer, and J. A. Pople, *Ab Initio Molecular Orbital Theory* (Wiley, New York, 1986), p. 25.
[17] D. R. Armstrong, P. G. Perkins, and J. P. Stewart, J. Chem. Soc. Dalton Trans. **1973**, 1044 (1973).
[18] A. A. Demkov, J. Ortega, O. F. Sankey, and M. P. Grumbach, Phys. Rev. B **52**, 1618 (1995).
[19] We caution the reader that the positions of unoccupied one-electron levels calculated with our method are not quantitatively

accurate. However, the one-electron level within the band gap is associated with a localized state, and the qualitative features displayed in Fig. 4 are expected to be correct.

[20] A. Hinchliffe, *Ab Initio Determination of Molecular Properties* (Hilger, Bristol, 1987).

[21] W. E. Carlos, Appl. Phys. Lett. **50**, 1450 (1987).

[22] M. Cook and C. T. White, Phys. Rev. B **38**, 9674 (1988).